# Centered reduced moments and associate density functions applied to alkaline comet assay

**Roman Castaneda**
Universidad Nacional de Colombia Sede Medellín
Physics School
Faculty of Science
A.A. 3840
Medellín, Colombia
E-mail: rcastane@perseus.unalmed.edu.co

**Alejandro Pelaez**
Universidad Nacional de Colombia Sede Medellín
Master of Biotechnology Program
Faculty of Science
A.A. 3840
Medellín, Colombia
and
Instituto de Ciencias de la Salud
Faculty of Dentistry
CES
Medellín, Colombia

**Maria-Elena Marquez**
Universidad Nacional de Colombia Sede Medellín
Master of Biotechnology Program
Faculty of Science
A.A. 3840
Medellín, Colombia

**Pablo Abad**
Universidad Nacional de Colombia Sede Medellín
Physics School
Faculty of Science
A.A. 3840
Medellín, Colombia

**Abstract.** The single cell gel electrophoresis assay is a sensitive, rapid, and visual technique for deoxyribonucleic acid (DNA) strand-break detection in individual mammalian cells, whose application has significantly increased in the past few years. The cells are embedded in agarose on glass slides followed by lyses of the cell membrane. Thereafter, damaged DNA strands are electrophoresed away from the nucleus towards the anode giving the appearance of a comet tail. Nowadays, charge coupled device cameras are attached at optical microscopes for recording the images of the cells, and digital image processing is applied for obtaining quantitative descriptors. However, the conventional software is usually expensive, inflexible and, in many cases, can only provide low-order descriptors based in image segmentation, determination of centers of mass, and Euclidean distances. Associated density functions and centered reduced moments offer an effective and flexible alternative for quantitative analysis of the comet cells. We will show how the position of the center of mass, the lengths and orientation of the main semiaxes, and the eccentricity of such images can be accurately determined by this method.  [DOI: 10.1117/1.1920567]

Keywords: SCGE assay; genotoxicity; centered reduced moments.

Paper 04073R received May 7, 2004; revised manuscript received Oct. 12, 2004; accepted for publication Nov. 11, 2004; published online May 24, 2005.

## 1 Introduction

The single cell gel electrophoresis (SCGE) assay has been successfully applied for genotoxic evaluation of many physical and chemical agents, such as ultraviolet-radiation,[1] x rays, $H_2O_2$, acrilamide,[2] oxidative stress in bovine embryo,[3] spermatic deoxyribonucleic acid (DNA) integrity,[4,5] and biocompatibility of biomaterials.[6]

The electrophoresis releases the segments of the broken strand of the damaged DNA in the surroundings outside of the cell. So, the appearance of the damaged DNA becomes similar to the tail of a comet, whose head is the nucleus of each single cell. By analyzing the microscope images, quantitative descriptors can be determined, which deal with the measurement of the local concentration of DNA molecules. Such a measurement is useful for clastogenicity diagnostic.

At the beginning, manual estimation of the comet features was attempted.[7] However, the time dependence of the fluorescence strongly limits the procedures respective to the reproducibility of the measurements and the error estimation. Very fast semiautomatic methods[8,9] that involve digital image acquisition and storing[10–12] overcome this limitation. Image processing routines for both real time and *a posteriori* analysis (i.e., image segmentation, determination of Euclidean distances, and centers of mass) has been implemented. Nevertheless, many of them can only provide low-order quantitative descriptors.

Distinguishing between the head and the tail on the image of the comet cell is crucial for an accurate quantitative estimation of their geometrical features.[13] Although high order moments of the light distribution of the comet image can be used to perform it, they are not effective in all cases, because their interpretation is usually very hard.

In this paper we will show that associated density functions and centered reduced moments provide high-order quantitative descriptors with well-defined geometric interpretations for both the head and the tail of the comet cells. Specifically, null, first and second order associated density functions were used for enhancing specific areas of the considered segment of the cell. Position of the centers of mass of such areas, length, and orientation of their semiaxes and their content of light intensity could be accurately determined from the centered reduced moments up to the sixth order.

Address all correspondence to Roman Castaneda, Physics School, Universidad Nacional de Colombia - Sede Medellín, AA.3840, MedellC-n, Antioquia Colombia. Tel: 57-4-4309370; Fax: 57-4-4309528; E-mail: rcastane@unalmed.edu.co

1083-3668/2005/$22.00 © 2005 SPIE

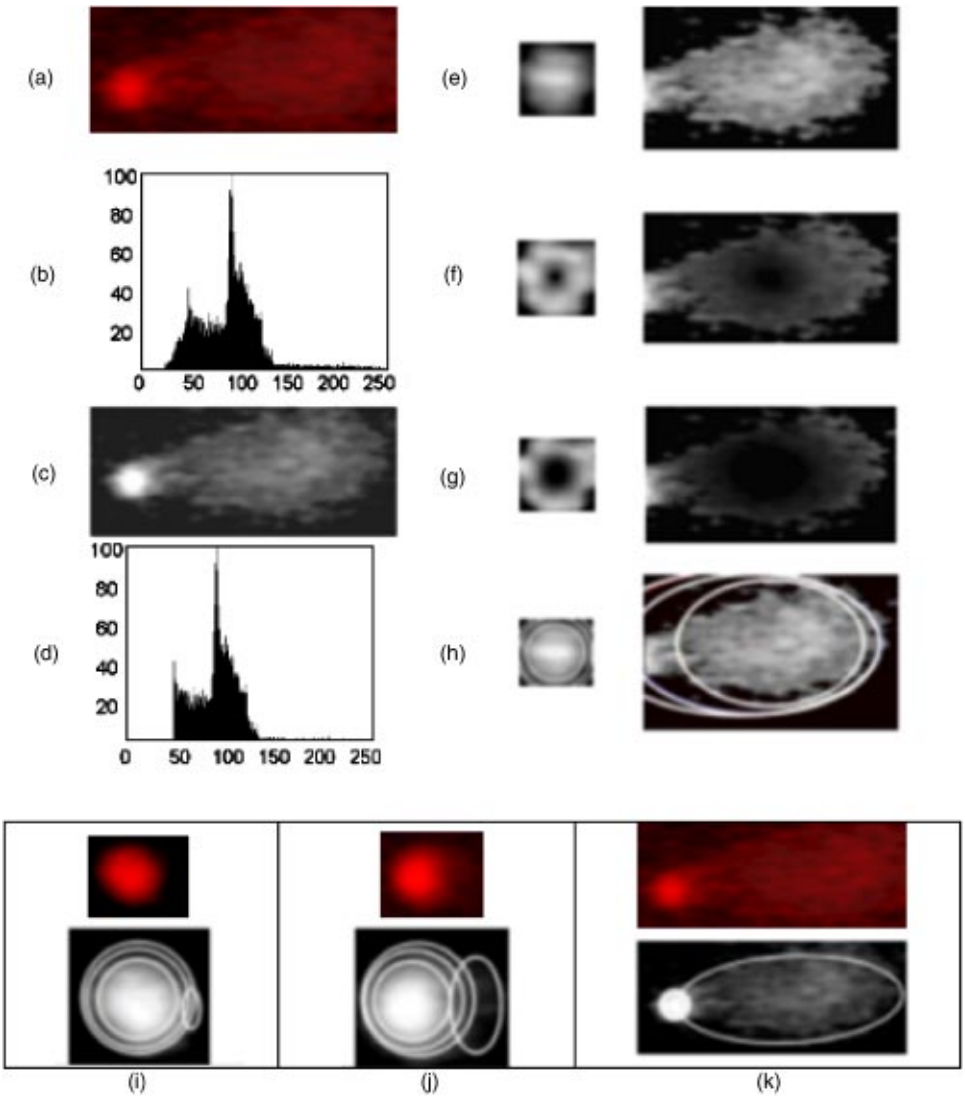


**Fig. 1** (a) Image of a comet cell acquired by a conventional CCD camera. (b) Gray-level histogram of this image. The vertical line points out the threshold value for noise suppression. (c) The same image after background noise suppression. (d) The gray-level histogram of the image after background noise suppression. (e) Head and tail of a comet cell in after the image segmentation. (f), (g) Associated density function ($i=0,1,2$) for the head and the tail of the comet cell. (h) Morphological descriptors of the head and the tail of the comet cell, the first ellipse inside together with its center is corresponding to $V_0(u,v)$, the second one to $V_1(u,v)$, and the third one to $V_2(u,v)$, with $u$ as the horizontal coordinate and $v$ as the vertical coordinate. (i), (j), (k) Showed cells with different states of cleavage of DNA and their respective morphological descriptors. Normal, softly, and strongly DNA damaged. (k) Image was reduced 1/3 the used scale in images (i) and (j).

So, these descriptors of the image intensity distribution can properly characterize the comet cells, and allow determining the DNA concentration by applying suitable proportionality rules.

## 2 Comet Cell Images Preprocessing

The images were obtained in a previous study designed to estimate the clastogenicity *in vitro*. The alkaline protocol for the SCGE assay, described by Singh et al.,[14] was applied on coatings of hybrid layers obtained by sol-gel containing glass, glass-ceramic, and HA particles on stainless steel AISI 304 in peripherical blood mononuclear cells.[15] Microscope images of comet cell were recorded by a conventional eight-bit charge coupled device (CCD) camera (i.e., 256 gray levels) attached at the epifluorescense optical microscope [Fig. 1(a)]. So, each image will be an array of $N \times M$ pixels, which can be represented by an $N \times M$ matrix of positive whole numbers, from 0 for black to 255 for white.

This matrix contains the information of the comet cell image superimposed onto a background of fluctuating low intensity values named background noise, which is mainly due to the dark currents in the CCD sensor.[10] This noise must be suppressed for accurately determining the high order moments of the image, because it strongly influences such moments. In fact, the higher the moment order the greater the significance of the noise values.[8]

In most cases, the values of the background noise are uniformly distributed onto the region of gray levels below the gray levels of the comet cell image. This region can be identified on the gray-level histogram as reported

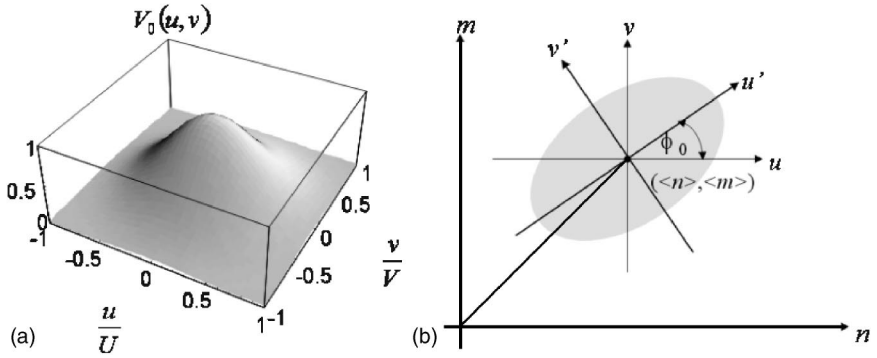


**Fig. 2** (a) $V_0(u,v)$ of an isolated cell nucleus in reduced coordinates. (b) Ellipse (shadowed area) determined by $\mu_{02}^{(0)}$, $\mu_{11}^{(0)}$, $\mu_{20}^{(0)}$.

previously,[10,16–18] so that its highest gray level can be used as a suitable threshold for background noise suppression [Fig. 1(b)].

The image gray levels under this threshold are set to null and those equal or greater than the threshold will remain unchanged. Thereafter, the threshold value will be subtracted from the unchanged image values to perform an offset reset.[10,17] The result is an image similar to that in Fig. 1(c), whose gray-level histogram is shown in Fig. 1(d).

Then, the comet image can be segmented into head and tail by applying a further threshold. Comet images show that the gray levels of the tail are not higher than the gray levels of the head. This means that the gray level corresponding to the main maximum of the gray-level histogram of the image provides the suitable threshold for segmentation, i.e., gray levels below it will correspond to the tail and those equal or greater than it will conform the head.

Thus, the head can be isolated by setting to null the gray levels greater than or equal to the threshold and applying the corresponding offset reset. The tail is isolated by setting to null the gray levels lower than the threshold and resetting the offset.

## 3 Centered Reduced Moments and Associated Density Functions

An image recorded by the CCD camera is numerically represented as a matrix of N×M elements with values $0 \leqslant f(n,m) \leqslant 255$. $(n,m)$ are pairs of whole numbers that label the pixel addresses, i.e., $0 \leqslant n \leqslant N-1$ and $0 \leqslant m \leqslant M-1$. Let us introduce the function $V_0(u,v)=f(u,v)/\|f\|$, with $u=n-\langle n\rangle$ and $v=m-\langle m\rangle$ called the *centered coordinates*, because $\langle n\rangle=(1/\|f\|)\Sigma_{n=0}^{N-1}\Sigma_{m=0}^{M-1} nf(n,m)$ and $\langle m\rangle=(1/\|f\|)\Sigma_{n=0}^{N-1}\Sigma_{m=0}^{M-1} mf(n,m)$ denote the position of the center of mass of the image, and $\|f\|=\Sigma_{n=0}^{N-1}\Sigma_{m=0}^{M-1} f(n,m)$ is the image energy content.

Thus, $V_0(u,v)$ exhibits the properties of the discrete density functions,[10,17] i.e., $V_0(u,v) \geqslant 0$, $\Sigma_{u=-U}^{U}\Sigma_{v=-V}^{V} V_0(u,v)=1$ and $V_0(u,v)\to 0$ for $(u,v)$ far away from the coordinate origin. Then, let us introduce its *centered reduced moments*[10,15] as follows:

$$\mu_{pq}^{(0)}=\sum_{u=-U}^{U}\sum_{v=-V}^{V}\left(\frac{u}{U}\right)^p\left(\frac{v}{V}\right)^q V_0(u,v), \qquad (1)$$

with $p \geqslant 0$ and $q \geqslant 0$ whole numbers, so that $p+q$ determines the order of the moments. Thus, there are $p+q+1$ centered reduced moments of order $p+q$. The term *reduced* is due to the fact that $-1 \leqslant u/U \leqslant 1$ and $-1 \leqslant v/V \leqslant 1$.

Low-order centered reduced moments provide a quantitative estimation of specific geometrical features of the image. Indeed, Eq. (1) yields $\mu_{00}^{(0)}=1$ and $\mu_{01}^{(0)}=\mu_{10}^{(0)}=0$ which denote the normalization of $V_0(u,v)$ and the position of its center of mass at the coordinate origin. The centered reduced moments of second order $\mu_{02}^{(0)}$, $\mu_{11}^{(0)}$, $\mu_{20}^{(0)}$ determine an ellipse of area $A_0$ that encloses the main intensity values of the image (Fig. 2). If $\mu_{11}^{(0)} \neq 0$ the semiaxis of the ellipse will be rotated with respect to the coordinate axis by an angle $\phi_0=\frac{1}{2}\arctan[2\mu_{11}^{(0)}/(\mu_{20}^{(0)}-\mu_{02}^{(0)})]$. After the rotation of $V_0(u,v)$ by $-\phi_0$, the semiaxis of the ellipse will be parallel to the coordinate axis and the centered reduced moments of second order will have new values $[\eta_{02}^{(0)},0,\eta_{20}^{(0)}]$.

Then, $a_0=\sqrt{\eta_{20}^{(0)}}$ and $b_0=\sqrt{\eta_{02}^{(0)}}$ will denote the lengths of the semiaxes of $V_0(u,v)$. Assuming $\eta_{02}^{(0)} \geqslant \eta_{20}^{(0)}$, i.e., $b_0 \geqslant a_0$, the eccentricity of the ellipse will be given by $E_0=\sqrt{1-(a_0/b_0)^2}=\sqrt{1-\eta_{20}^{(0)}/\eta_{02}^{(0)}}$, so that $0 \leqslant E_0 \leqslant 1$. The condition $\eta_{02}^{(0)}=\eta_{20}^{(0)}$ implies $a_0=b_0$ and $E_0=0$. Consequently, $V_0(u,v)$ will be circular symmetric, i.e., $\eta_{02}^{(0)}=\eta_{20}^{(0)}=\mu_{02}^{(0)}=\mu_{20}^{(0)}$ and $\eta_{11}^{(0)}=\mu_{11}^{(0)}=0$. In practical applications $V_0(u,v)$ can be regarded as circular symmetric if the condition $a_0 \geqslant 0.9b_0$ holds, i.e., $E_0 \leqslant 0.4359$. On the other hand, $E_0=1$ is obtained if $\eta_{20}^{(0)}=0$. It means that the rotated $V_0(u,v)$ is concentrated along a straight-line parallel to the $v$ axis, because $a_0=0$.

Furthermore, the fraction of the image energy enclosed by the ellipse is given by $E_0=\Sigma_{(u,v)\in A_0} V_0(u,v)$. It is customary to perform further analysis based on higher order moments if $E_0 \leqslant 0.8$.[10,17,18] However, geometric descriptors based on higher order moments are not straightforwardly defined at all.

To overcome this limitation, we define the *associated density functions*[10,15] as

$$V_i(u,v)=C_i\left[\left(\frac{u}{U}\right)^2+\left(\frac{v}{V}\right)^2\right]^i V_0(u,v), \qquad (2)$$

with $i=0, 1, 2,...$ and $C_i$ a constant that assures the normalization condition $\mu_{00}^{(i)}=\Sigma_{u=-U}^{U}\Sigma_{v=-V}^{V} V_i(u,v)=1$, i.e., $C_0=1$, $C_1=1/[\mu_{20}^{(0)}+\mu_{02}^{(0)}]$, $C_2=1/[\mu_{40}^{(0)}+2\mu_{22}^{(0)}+\mu_{04}^{(0)}]$, and

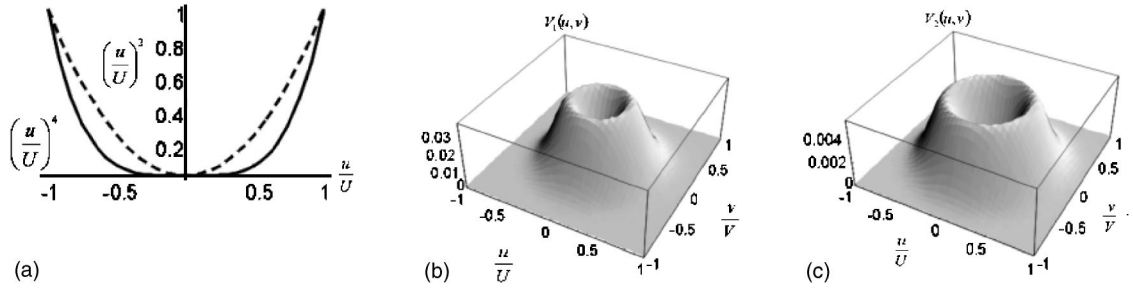


**Fig. 3** (a) Profiles of $(u/U)^2+(v/V)^2$ and $[(u/U)^2+(v/V)^2]^2$ for $v=0$. (b) $V_1(u,v)$ and (c) $V_2(u,v)$ associated to the isolated cell nucleus in Fig. 2.

so on. The coefficient $[(u/U)^2+(v/V)^2]^i$ for $i>0$ determines revolution surfaces, which take the value null at the origin [center of mass of $V_0(u,v)$] and one at the edges of the image area [Fig. 3(a)]. As a consequence, this coefficient strongly diminishes the values of $V_0(u,v)$ in a vicinity of its center of mass, whereas enhances the values of $V_0(u,v)$ outside of such a vicinity, as depicted in Figs. 3(b) and 3(c). Table 1 shows the first and second order centered reduced moments of the associated density functions for $i=0$, 1, 2 in terms of the centered reduced moments of $V_0(u,v)$ up to the sixth order.

It is well known that all the odd order moments of $V_0(u,v)$ are equal to null if the image is symmetric with respect to the coordinates origin.[17,18] Therefore, the centers of mass of $V_0(u,v)$, $V_1(u,v)$, and $V_2(u,v)$ will coincide in this case, i.e., $\mu_{01}^{(1)}=\mu_{10}^{(1)}=\mu_{01}^{(2)}=\mu_{10}^{(2)}=0$. Otherwise, the image asymmetries with respect to the coordinate origin can be estimated by the vectors

**Table 1** First and second order reduced moments of the associated density functions in terms of the centered reduced moments of $V_0(u,v)$ up to the sixth order. The expressions for the second order moments are valid for symmetric associated density functions.

| Moments | $i=0\rightarrow V_0(u,v)$ | $i=1\rightarrow V_1(u,v)$ | $i=2\rightarrow V_2(u,v)$ |
|---|---|---|---|
| $\mu_{01}^{(i)}$ | 0 | $\frac{\mu_{21}^{(0)}+\mu_{03}^{(0)}}{\mu_{20}^{(0)}+\mu_{02}^{(0)}}$ | $\frac{\mu_{41}^{(0)}+2\mu_{23}^{(0)}+\mu_{05}^{(0)}}{\mu_{40}^{(0)}+2\mu_{22}^{(0)}+\mu_{04}^{(0)}}$ |
| $\mu_{10}^{(i)}$ | 0 | $\frac{\mu_{30}^{(0)}+\mu_{12}^{(0)}}{\mu_{20}^{(0)}+\mu_{02}^{(0)}}$ | $\frac{\mu_{50}^{(0)}+2\mu_{32}^{(0)}+\mu_{14}^{(0)}}{\mu_{40}^{(0)}+2\mu_{22}^{(0)}+\mu_{04}^{(0)}}$ |
| $\mu_{02}^{(i)}$ | $\mu_{02}^{(0)}$ | $\frac{\mu_{40}^{(0)}+\mu_{22}^{(0)}}{\mu_{20}^{(0)}+\mu_{02}^{(0)}}$ | $\frac{\mu_{42}^{(0)}+2\mu_{24}^{(0)}+\mu_{06}^{(0)}}{\mu_{40}^{(0)}+2\mu_{22}^{(0)}+\mu_{04}^{(0)}}$ |
| $\mu_{11}^{(i)}$ | $\mu_{11}^{(0)}$ | $\frac{\mu_{31}^{(0)}+\mu_{13}^{(0)}}{\mu_{20}^{(0)}+\mu_{02}^{(0)}}$ | $\frac{\mu_{51}^{(0)}+2\mu_{33}^{(0)}+\mu_{15}^{(0)}}{\mu_{40}^{(0)}+2\mu_{22}^{(0)}+\mu_{04}^{(0)}}$ |
| $\mu_{20}^{(i)}$ | $\mu_{20}^{(0)}$ | $\frac{\mu_{22}^{(0)}+\mu_{04}^{(0)}}{\mu_{20}^{(0)}+\mu_{02}^{(0)}}$ | $\frac{\mu_{60}^{(0)}+2\mu_{42}^{(0)}+\mu_{24}^{(0)}}{\mu_{40}^{(0)}+2\mu_{22}^{(0)}+\mu_{04}^{(0)}}$ |

$$\mathbf{D}_1=\mu_{10}^{(1)}\hat{\mathbf{u}}_x+\mu_{01}^{(1)}\hat{\mathbf{u}}_y=\frac{1}{\mu_{20}^{(0)}+\mu_{02}^{(0)}}\{[\mu_{21}^{(0)}+\mu_{03}^{(0)}]\hat{\mathbf{u}}_x+[\mu_{30}^{(0)}+\mu_{12}^{(0)}]\hat{\mathbf{u}}_y\} \tag{3a}$$

for asymmetric $V_1(u,v)$ and

$$\mathbf{D}_2=\mu_{10}^{(2)}\hat{\mathbf{u}}_x+\mu_{01}^{(2)}\hat{\mathbf{u}}_y=\frac{1}{\mu_{40}^{(0)}+2\mu_{22}^{(0)}+\mu_{04}^{(0)}}\{[\mu_{41}^{(0)}+2\mu_{23}^{(0)}+\mu_{05}^{(0)}]\hat{\mathbf{u}}_x+[\mu_{50}^{(0)}+2\mu_{32}^{(0)}+\mu_{14}^{(0)}]\hat{\mathbf{u}}_y\} \tag{3b}$$

for asymmetric $V_2(u,v)$. In practical situations, images can be regarded as symmetric with respect to the coordinate origin [center of mass of $V_0(u,v)$] if the condition $|\mathbf{D}_i|\leqslant 0.2a_0$ is fulfilled, with i=1, 2 and $a_0$ as the minor semiaxis of $V_0(u,v)$.

The length and orientation of the semiaxes and the eccentricities of the associated density functions are determined from their second order centered reduced moments. For $V_1(u,v)$ these moments are given by

$$\mu_{p,2-p}^{(1)}=\frac{\mu_{2+p,2-p}^{(0)}+\mu_{p,4-p}^{(0)}}{\mu_{20}^{(0)}+\mu_{02}^{(0)}}+\sum_{n=0}^{3}\sum_{m=0}^{3}A_{nm}[\mu_{10}^{(1)}]^n[\mu_{01}^{(1)}]^m, \tag{4a}$$

and for $V_2(u,v)$ by

$$\mu_{p,2-p}^{(2)}=\frac{\mu_{p+4,2-p}^{(0)}+2\mu_{p+2,4-p}^{(0)}+\mu_{p,6-p}^{(0)}}{\mu_{40}^{(0)}+2\mu_{22}^{(0)}+\mu_{04}^{(0)}}+\sum_{n=0}^{6}\sum_{m=0}^{6}B_{nm}[\mu_{10}^{(2)}]^n[\mu_{01}^{(2)}]^m, \tag{4b}$$

with p=0, 1, 2. The coefficients $A_{nm}$ depend in general on the centered reduced moments of $V_0(u,v)$ of order lower than 4, and $B_{nm}$ on those whose order is lower than 6. Their specific forms are obtained by applying the definition of the second order centered reduced moments.

They can also take the values null and one. By example, for $\mu_{02}^{(1)}$ we obtain $A_{02}=1$ and all the reminded $A_{nm}$ are equal to null, whereas $A_{20}=1$ and all the reminded $A_{nm}$ are equal to null for $\mu_{20}^{(1)}$. But for $\mu_{11}^{(1)}$, the coefficients $A_{0,m>0}$, $A_{n>0,0}$, and $A_{11}$ will be different from both null and one. All the reminded ones will be equal to null. A similar analysis can be

**Table 2** Centered reduced moments $\mu_{pq}^{(0)}$ up to the fourth order for the comet cell in Fig. 1.

| | Head | | | | | Tail | | | | |
|---|---|---|---|---|---|---|---|---|---|---|
| p \ q | 0 | 1 | 2 | 3 | 4 | 0 | 1 | 2 | 3 | 4 |
| 0 | | 58.34 | 683.12 | 148.24 | 0.00 | | 165.87 | 886898.58 | 54283.24 | 560.00 |
| 1 | 65.08 | −21.33 | −23.05 | 0.00 | | 185.60 | −84988.65 | 2378.41 | 317.16 | |
| 2 | 628.09 | 37.46 | 0.00 | | | 344067.08 | 22451.72 | 179.62 | | |
| 3 | −18.17 | 0.00 | | | | 1416.07 | 101.73 | | | |
| 4 | 0.00 | | | | | 560.00 | | | | |

performed in Eq. (4b). On the other hand, note that the second terms on the right side of Eqs. (4a) and (4b) depend on powers of the centered reduced moments of first order of $V_1(u,v)$ and $V_2(u,v)$, respectively, i.e., the coordinates of the corresponding centers of mass. Thus, these terms do not appear if the associated density functions are symmetric with respect to the origin of coordinates because $\mu_{01}^{(i)}=\mu_{10}^{(i)}=0$ in these cases. Consequently, Eqs. (4a) and (4b) yield the expressions in Table 1 for the second order centered reduced moments of symmetric associated density functions.

The centered reduced moments $\mu_{02}^{(i)}$, $\mu_{11}^{(i)}$, and $\mu_{20}^{(i)}$ (i $=0,1,2$) determine an ellipse of area $A_i$, centered at the center of mass of $V_i(u,v)$, that encloses the main values of the corresponding associated density function. The semiaxes of such ellipses will be rotated respective to the coordinate axes by angles $\phi_i=\frac{1}{2}\arctan\{2\mu_{11}^{(i)}/[\mu_{20}^{(i)}-\mu_{02}^{(i)}]\}$. Then, a rotation of the corresponding associated density function by $-\phi_i$ will set their semiaxes parallel to the coordinate axes, allowing an accurate determination of their lengths and the eccentricity of the associated density function. After such rotations, the second order centered reduced moments of the associated density functions will take new values $[\eta_{02}^{(i)},0,\eta_{20}^{(i)}]$. Thus, the lengths of the semiaxes and the eccentricities of the ellipses will be given by

$$a_i=\sqrt{\eta_{20}^{(i)}}, \tag{5a}$$

$$b_i=\sqrt{\eta_{02}^{(i)}}, \tag{5b}$$

and

$$E_i=\sqrt{1-\left(\frac{a_i}{b_i}\right)^2}=\sqrt{1-\frac{\eta_{20}^{(i)}}{\eta_{02}^{(i)}}}, \tag{5c}$$

respectively, assuming $\eta_{02}^{(i)}\geqslant\eta_{20}^{(i)}$, i.e., $b_i\geqslant a_i$, so that $0\leqslant E_i\leqslant 1$. The condition $\eta_{02}^{(i)}=\eta_{20}^{(i)}$ implies $a_i=b_i$ and $E_i=0$. Consequently, $V_i(u,v)$ will be circular symmetric, i.e., $\eta_{02}^{(i)}=\eta_{20}^{(i)}=\mu_{02}^{(i)}=\mu_{20}^{(i)}$ and $\eta_{11}^{(i)}=\mu_{11}^{(i)}=0$. In practical applications $V_i(u,v)$ can be regarded as circular symmetric if the condition $a_i\geqslant 0.9b_i$ holds, i.e., $E_i\leqslant 0.4359$. Furthermore, $E_i=1$ is obtained if $\eta_{20}^{(i)}=0$, that is if the associated density function concentrates along a straight-line parallel to the $v$ axis.

Now, the fraction of the energy content of the image enclosed by each ellipse is given by

$$\mathsf{E}_i=\sum_{(u,v)\in A_i} V_0(u,v). \tag{6}$$

It is expected that $\mathsf{E}_{i+1}\geqslant\mathsf{E}_i$ (i=0,1,2...) because $A_{i+1}\geqslant A_i$. Furthermore, $\mathsf{E}_2\geqslant 0.8$ usually holds for the comet cell images we are concerned with. It justifies the statement that the set of centered reduced moments up to the sixth order provides an accurate and exhaustive description of the features of such images. Obviously, if $\mathsf{E}_2<0.8$, associated density functions of higher order must be introduced for properly achieving the image analysis.

In summary, associated density functions allow an accurate geometrical characterization of images based on centered reduced moments of high orders and on the few descriptors they determine (i.e., position of their centers of mass, lengths, and orientations of their semiaxis and their eccentricity).

Centered reduced moments of a specific order are related to a specific associated density function, so that the segments of the image they determine will be separately characterized. The enclosed energy fraction provides a criterion to establish the highest order required to perform an effective analysis.

## 4 Results

To illustrate the earlier procedure, let us consider the comet cell image in Fig. 1, which was split into head and tail. The electrophoresis device was prepared in such a way that the uniform electrical field was applied parallel to the coordinate axis u (horizontal axis in the images), and therefore orthogonal to the v axis (vertical axis in the images).

Table 2 shows the centered reduced moments $\mu_{pq}^{(0)}$ up to the fourth order for the head and the tail, respectively. The convergence of the moments is apparent in both cases, i.e., their values significantly decrease when the order increases. It means that the information we are looking for can be exhaustively provided by a finite and small number of centered reduced moments. Fourth order moments of the head are essentially equal to null because the corresponding coefficients $(u/U)^p(v/V)^q$, for $\mathsf{p}+\mathsf{q}=4$, screen the relevant information of the head.

**Table 3** Morphological descriptors for the comet in Fig. 1.

| | | Head | | | | | | Tail | | | | | |
|---|---|---|---|---|---|---|---|---|---|---|---|---|---|
| DNA | Descriptors | $V_0(u,v)$ | | $V_1(u,v)$ | | $V_2(u,v)$ | | $V_0(u,v)$ | | $V_1(u,v)$ | | $V_2(u,v)$ | |
| Normal | Center of mass position $(u,v)$ | 0.00 | 0.00 | −0.11 | 0.04 | −1.13 | −1.56 | 53.54 | 18.32 | 53.46 | 18.69 | 53.44 | 19.43 |
| | Length of the semiaxes in $\mu$m | 5.52 | 5.59 | 6.93 | 7.07 | 7.78 | 7.90 | 2.76 | 1.25 | 4.33 | 1.14 | 5.03 | 1.20 |
| | Eccentricity | 0.11 | | 0.14 | | 0.12 | | 0.00 | | 0.00 | | 0.00 | |
| | Energy content | 88.94 | | 99.36 | | 99.95 | | 81.27 | | 96.57 | | 97.66 | |
| Softly affected | Center of mass position $(u,v)$ | 0.00 | 0.00 | −0.12 | 0.66 | −1.67 | −1.96 | 50.13 | 19.90 | 50.23 | 20.76 | 51.01 | 21.63 |
| | Length of the semiaxes in $\mu$m | 6.83 | 6.76 | 8.78 | 8.62 | 9.91 | 9.76 | 8.40 | 4.01 | 12.07 | 3.76 | 13.25 | 4.42 |
| | Eccentricity | 0.10 | | 0.13 | | 0.12 | | 0.72 | | 0.83 | | 0.82 | |
| | Energy content | 88.06 | | 91.96 | | 92.95 | | 86.87 | | 90.80 | | 91.95 | |
| Strongly affected | Center of mass position $(u,v)$ | 0.00 | 0.00 | 0.00 | 0.00 | 0.00 | 0.00 | 4.05 | 4.05 | 4.05 | 4.05 | 4.05 | 4.05 |
| | Length of the semiaxes in $\mu$m | 3.36 | 3.52 | 4.29 | 4.51 | 4.79 | 5.08 | 17.95 | 27.02 | 19.82 | 36.88 | 20.51 | 40.45 |
| | Eccentricity | 0.22 | | 0.22 | | 0.24 | | 0.58 | | 0.68 | | 0.70 | |
| | Energy content | 88.21 | | 99.35 | | 99.95 | | 82.33 | | 83.13 | | 84.54 | |

Table 3 shows the morphological descriptors of such comet cell, which are represented by the central points and the ellipses in Figs. 1(i), 1(j), and 1(k). As expected, the displacement of the centers of mass along the direction of the applied electrical field in the strongly affected cell is more significantly than along the $v$ axis (vertical axis). However, these displacements are shorter in the cell head as in the cell tail. It means that DNA molecules remain concentrated around the nucleus in head, but they are nonsymmetrically distributed onto an extended region in the tail. In addition, the eccentricity is smaller than 0.24 for the head and greater than that for the tail. Therefore, the head essentially exhibits circular symmetry, but the tail distributes onto an elliptical region as confirmed by the lengths of the semiaxes. Indeed, the horizontal semiaxis of the tail is bigger than the vertical one because of the orientation of the electrical field. Furthermore, the percent of the energy content corresponding to the above descriptors were greater than 81.27% of the total energy of the respective images. It allows us to state that such descriptors accurately characterize the cell features of interest.

Cells with nondamaged DNA [Fig. 1(i)] are circular symmetric at all, so that the associated density functions of the cell nucleus yield concentric circles. As the analysis for the tail is performed, a small ellipse is generated. However, its center of mass is practically located at the nucleus membrane, its minor semiaxis is parallel to the electrical field direction, its length will be significantly smaller than the nucleus radius, and its major semiaxis will be also smaller than the nucleus radius but orthogonal to the electrical field direction. Therefore the structure identified by the tail analysis will be in fact a halo around the cell but not a comet tail. This analysis is confirmed by the corresponding numerical results in Table 3.

Cells with softly affected DNA [Fig. 1(j)] remains circular symmetric, but the centers of mass of its associated density functions will be displaced to each other. The major semiaxis of the tail ellipse remains orthogonal to the electric field direction but its length is now comparable to the nucleus diameter. Furthermore, the center of mass of this ellipse lies at a certain distance of the nucleus membrane. That means that DNA molecules migrate outside the cell through the mem-

**Table 4** Differences between the descriptors given by CSS and CRM&ADF for Fig. 1. CS—comet score software, CRM&ADF—centered reduced moments and associate density functions, and P.E.—Percent error relative to CSS. Calculated with, P.E.=(CRM&ADF−CSS)/CSS×100.

| | | Comet length | | Comet height | | Head area | | Tail length | | Tail area | |
|---|---|---|---|---|---|---|---|---|---|---|---|
| DNA | Method | ($\mu$m) | P.E. | ($\mu$m) | P.E. | ($\mu m^2$) | P.E. | ($\mu$m) | P.E. | ($\mu m^2$) | P.E. |
| Normal | CSS | 12.90 | −10.36 | 11.55 | −5.70 | 106.25 | 154.42 | 0.37 | 36.22 | 5.81 | −58.88 |
| | CRM&ADF | 11.56 | | 10.89 | | 270.32 | | 0.50 | | 2.39 | |
| Softly affected | CSS | 20.88 | −19.74 | 17.32 | 7.10 | 187.63 | 126.72 | 5.90 | −47.56 | 65.85 | 95.58 |
| | CRM&ADF | 16.76 | | 18.55 | | 425.40 | | 3.09 | | 128.79 | |
| Strongly affected | CSS | 70.64 | −17.78 | 31.45 | −8.70 | 104.65 | 2.27 | 54.18 | −5.93 | 1053.79 | 211.64 |
| | CRM&ADF | 58.08 | | 28.71 | | 107.02 | | 50.97 | | 3284.01 | |

brane, although a significant concentration of DNA even remains inside the cell. Thus, the cell exhibits a relative small comet tail.

To compare the performance of the proposed method [centered reduced moments and associated density functions (CRM&ADF)] with a conventional procedure, we have applied the ''comet score'' free software (CSS) to the same comet cells in Figs. 1(i), 1(j), and 1(k). The noise threshold was fixed at 0.94 and the magnification was calibrated by means of the micrometric grid of a hemocytometer.

Table 4 shows the percent differences between the results given by two methods (CSS and CRM&ADF). The values of the comet heights are close similar. Probably, the small absolutes differences (<8.7%) are related to the threshold value chosen by the user of the CSS.

Bigger differences were obtained in the estimation of the head area in Figs. 1(i) and 1(j). They can be attributed to the better processing of diffuse borders of CRM&ADF method. Indeed, other methods usually consider the concept of ''extent head'' in the analysis of the cell head, which neglect the values close to the diffuse borders. A similar reason explains the differences in the estimation of the tail length. However, the tail areas estimated by CRM&ADF method are not determined by the pixels of the tails in the images, but by mathematical ellipses determined by the tail descriptors. Therefore their values are greater than the size of the regions occupied by the pixels.

## 5 Conclusion

Image processing based on centered reduced moments and associated density functions constitutes an effective tool for quantitative characterization of comet cells from SCGE assay. It could be separately applied to the nucleus and the tail of the comet and also perform a global evaluation of the cell. By using relative simple software, exhaustive evaluation is performed by calculating high order moments.

### *Acknowledgments*

This study was supported by the DIME (Universidad Nacional de Colombia—Sede Medellín) and Instituto Colombiano para el Desarrollo de la Ciencia y la Tecnología (Colciencias) Grant No. 1118-12-13724.

### *References*

1. M. H. Green, J. E. Lowe, S. A. Harcourt, P. Akinluyi, T. Rowe, J. Cole, A. V. Anstey, and C. F. Arlett, ''UV-C sensitivity of unstimulated and stimulated human lymphocytes from normal and xeroderma pigmentosum donors in the comet assay: a potential diagnostic technique,'' *Mutat Res.* **273**, 137–144 (1992).
2. R. Tice, J. Chaillet, and E. L. Schneider, ''Demonstration of spontaneous sister chromatid exchanges *in vivo*,'' *Exp. Cell Res.* **102**, 426–429 (1976).
3. M. Takahashi, K. Keicho, H. Takahashi, H. Ogawa, R. M. Schultz, and A. Okano, ''Effect of oxidative stress on development and DNA damage in *in-vitro* cultured bovine embryos by comet assay,'' *Theriogenology* **54**, 137–145 (2000).
4. G. A. Haines, J. H. Hendry, C. P. Daniel, and I. D. Morris, ''Increased levels of comet-detected spermatozoa DNA damage following in vivo isotopic- or X-irradiation of spermatogonia,'' *Mutat Res.* **495**, 21–32 (2001).
5. C. M. Hughes, S. E. Lewis, V. J. McKelvey-Martin, and W. Thompson, ''The effects of antioxidant supplementation during Percoll preparation on human sperm DNA integrity,'' *Hum. Reprod.* **13**, 1240–1247 (1998).
6. D. J. Chauvel-Lebret, P. Auroy, S. Tricot-Doleux, and M. Bonnaure-Mallet, ''Evaluation of capacity of the SCGE assay to assess the genotoxicity of biomaterials,'' *Biomaterials* **22**, 1795–1801 (2001).
7. C. Helma and M. Uhl, ''A public domain image-analysis program for the single-cell gel-electrophoresis (comet) assay,'' *Mutat Res.* **3**(466), 9–15 (2000).
8. R. Castañeda and J. C. Correa, ''A simple method for analyzing the tails of distributions,'' *Rev. Acad. Col. Cie. Exact., Fis y Nat.* **89**, 555–562 (1999).
9. B. Hellman, H. Vaghef, and B. Bostrom, ''The concepts of tail moment and tail inertia in the single cell gel electrophoresis assay,'' *Mutat Res.* **336**, 123–131 (1995).
10. R. Castañeda, ''Two dimensional evaluation of point spread functions using centered reduced moments,'' *Pure Appl. Opt.* **3**, 737–755 (1994).
11. W. Bocker, T. Bauch, W. U. Muller, and C. Streffer, ''Image analysis of comet assay measurements,'' *Int. J. Radiat. Biol.* **72**, 449–460 (1997).

12. P. J. McCarthy, S. F. Sweetman, P. G. McKenna, and V. J. McKelvey-Martin, ''Evaluation of manual and image analysis quantification of DNA damage in the alkaline comet assay,'' *Mutagenesis* **12**, 209–214 (1997).
13. K. Konca, A. Lankoff, A. Banasik, H. Lisowska, T. Kuszewski, S. Gozdz, Z. Koza, and A. Wojcik, ''A cross-platform public domain PC image-analysis program for the comet assay,'' *Mutat Res.* **534**, 15–20 (2003).
14. N. P. Singh, ''Microgels for estimation of DNA strand breaks, DNA protein crosslinks and apoptosis,'' *Mutat Res.* **455**, 111–127 (2000).
15. A. Pelaez, A. Pareja, C. P. Garcia, M. E. Márquez, A. Toro, R. Castañeda, and P. Abad, ''Genotoxicity efects of ceramic coatings applied on metallic substrates using single cell gel electrophoresis assay *in vitro*,'' *Key Eng. Mater.* **284**, 593–596 (2005).
16. R. González and R. E. Woods, *Digital Image Processing*, Addison-Wesley, Reading, MA (1992).
17. R. Castañeda, J. García, and F. Brand, ''Quality descriptors of optical beams based on centered reduced moments I: Spot analysis,'' *Opt. Commun.* **227**, 37–48 (2003).
18. R. Castañeda, J. García, and F. Brand, ''Quality descriptors of optical beams based on centered reduced moments II: Retrieving of the complex degree of spatial coherence through the spot moments,'' *Opt. Commun.* **238**, 191–200 (2004).